Defence Science Journal, Vol. 66, No. 4, July 2016, pp. 291-306, DOI : 10.14429/dsj.66.10203

REVIEW ARTICLE

A Novel Method for the Synthesis of Core-shell Magnetic Nanoparticle

D. Mukherji

Technische Universität Braunschweig, Institut für Werkstoffe, DE-38106 Braunschweig, Germany
E-mail:d.mukherji@t-online.de

ABSTRACT

Core-shell type magnetic nanoparticles are finding attractive applications in biomedicine, from diagnostic to cancer therapy. Both for targeted drug delivery and hyperthermia, as well as a contrast agent used for external biomedical imaging systems, small (< 20 nm) superparamagnetic nanoparticles are desired. Some iron oxide nanoparticle formulations are already approved for human administration as contrast agent for magnetic resonance imaging. However, search continues for nanoparticles with higher saturation magnetisation. Metallic, bi-metallic and intermetallic magnetic nanoparticles are finding attention. Biocompatibility and optimal *clearance* are important criteria for the medical applications and therefore core-shell type particles are favoured, where a biocompatible shell (e.g. polymer, Silica) can prevent inadvertent host reaction with the magnetic core. A recently developed novel synthesis method (electrochemical selective phase dissolution - ESPD), which can produce core-shell magnetic nanoparticles, is reviewed. ESPD, as the name suggests, uses electro-chemical separation of a phase from metallic alloys to synthesise nanoparticles. It is a versatile method and can be adopted to produce a wide range of nanostructures in addition to the core-shell magnetic nanoparticles.

Keywords: Magnetic nanoparticles, core-shell, drug-delivery, hyperthermia, nano-templates

1. INTRODUCTION

Nanoscale research, on a length scale of 1 to 100 nanometers, refers to science, engineering, and technology at the level of atoms and molecules. Whereas nano science involves the study and comprehension of nature at this scale, nanotechnology intends the direct application of nano science for the development of new products and techniques. Functionalised nanoparticle with controllable sizes is one of the very important recent development, as their very small size places them at dimensions that are smaller than or comparable to those of a cell (10 μm – 100 μm), a virus (20 nm – 450 nm), a protein (5 nm – 50 nm) or a gene (2 nm wide and 10 nm – 100 nm long) – i.e. close to a biological entity of interest. Thus, amongst many disciplines, the development of nanotechnology is greatly affecting biotechnology and medicine. Magnetic nanoparticles (MNP), in particular offer new attractive possibilities in biomedicine.

The nanoscale is the scale at which the fundamental properties of materials are established. Much is known about the physical properties and behaviour of bulk materials and isolated molecules, however, the properties of matter at the nanoscale cannot necessarily be predicted just by scaling down. Instead, they exhibit important differences that cannot be explained by traditional models and theories. The first, very important, property of nanoparticles is their large surface-to-volume ratio which makes them distinct from larger particles. As the size of the particles becomes smaller to nanoscale, the number of atoms near the surface of the particle becomes comparable to that in the volume. As a consequence, the physical properties of nanoparticles differ significantly from macroscopic and even microscopic one on reducing their size. Actually, matter at the nanoscale does not satisfy the laws of classical physics anymore because quantum effects become predominant. Nanoparticles have attracted much attention because of their associated physical attributes, which are different from their bulk counterparts. Such changes due to only size reduction can affect many physical, mechanical, electrical, optical and magnetic properties[1]. For example, both the orbital and the spin moments on the surface of tiny magnetic nanoparticles are strongly enhanced. This is a consequence of the fact that a high number of atoms with lower coordination number sit on the surface and therefore exhibit uncompensated (spin) distributions of magnetic moments[2].

Nanostructured materials, and in particular MNPs, are finding increasing applications in chemistry, biomedicine, electronics and materials engineering. The use of materials at the nanoscale, specifically magnetic nanoparticles, is currently a prominent topic in healthcare and life science. Due to their size-tunable physical and chemical properties, MNPs have attracted considerable interest for a wide range of applications ranging from medical diagnosis to cancer treatment. Advances in nanotechnology and molecular biology are rapidly enabling the development of nanoparticles with specific functionality that addresses the shortcomings of traditional disease diagnostic and therapeutic agents[3]. Multi-functional MNPs are gaining importance, and nanoparticles formed as core-shell type structure by surface modification have emerged as an important class of functional nanomaterial. Core–shell nanoparticles with magnetic core capped with an inert biocompatible shell are intensively studied as they are candidates for medical

Received : 23 January 2016, Revised : 03 March 2016
Accepted : 06 June 2016, Online published : 28 June 2016

applications like magnetic hyperthermia and targeted drug delivery[4].

In many applications, nanoparticles with a core–shell structure are preferred because in the core–shell particles, the center and the surface region have different structure and/or composition and therefore can be tuned to different properties. These are systems of special interest from the point of view of both production and application. A shell can be formed either naturally during the particle production process or during their use, or deliberately through processing. In the later case, a shell structure is purposefully produced around the nanoparticles, either to change their physico-chemical properties, or to adapt them to the environment in which they are to be used. For example, in bi-layer metal nanoparticles a shell can change the optical properties of a colloidal dispersion; in these cases the optical absorption can be tuned by choosing the capping material and its thickness[5]. Another example is that of magnetic nanoparticles used for drug delivery, which are covered with polymeric materials[4]. In particular, covering metal nanoparticles by inert shell material (e.g. silica or oxide) is a common practice, which is adopted for colloidal suspensions[6]. In these cases, the inert shell prevents coagulation of particles through chemical stabilisation, without changing the optical, electrical or magnetic properties of the core.

A variety of physical and chemical methods have been employed to synthesise nanoparticles of semiconductors, metals, oxides and rare earth metals[7,8]. The different techniques include synthesis of nanoparticles using vacuum, gas-phase or condensed-phase processing. Main methods are sputtering, laser ablation, inert gas condensation, etc. Nanoparticles may also be produced by mechanical alloying or other means of severe plastic deformation[9], or by chemical methods such as reduction reactions and wet chemical processes[10,11]. Various methods, both physical and chemical, can also be used to produce core–shell nanoparticles. Generally, these methods need two steps—first the core particle is produced and then it is covered by the shell material in a second step of the manufacturing process[12]. A novel process to produce nanoparticles of intermetallic phases from simple two-phase metallic alloys has been recently developed[13]. In this process, nano sized precipitates of intermetallic phases are grown in a bulk metallic alloy to the desired size and shape, and later they are extracted by electrochemical selective phase dissolution (ESPD) of the matrix[14]. This process can be also adopted to produce core-shell magnetic nano particles in one step[15].

Some general criteria of nanoparticle design for targeted drug delivery, imaging and hyperthermia. Then review the synthesis and characterisation of nanoparticles produced by ESPD, including in particular the core-shell MNPs. Finally, shows the versatility of the ESPD process, which can be adopted for the production of other nano-structured materials, e.g. nano-porous membrane or nano-templates.

2. NANOPARTICLE DESIGN CONSIDERATIONS FOR BIOMEDICAL APPLICATIONS

Depending on particle size, composition, structure and physico-chemical properties, MNPs have demonstrated a diverse range of useful applications from magnetic resonance imaging (MRI), hyperthermia, separation or drug-delivery to catalysis[16–19]. However, to be effective in diagnostic and therapy the MNPs must fulfill certain criteria. For targeted drug delivery or hyperthermia, as well as a contrast agent used in an external biomedical imaging system, the nanoparticles must be able to navigate the human body and selectively attach to target cells or tissues and play their therapeutic role or enhance tissue contrast in MRI. In doing so it must be a biocompatible entity that will not harm the patient or the healthy tissues. Radiotherapy (radiation therapy) and chemotherapy are based on the use of ionising radiation to control or kill cancer cells. Cancer cells show an increased metabolism and divide rapidly. Their enhanced radio sensitivity as compared to normal cells makes them more vulnerable to radiation or cytotoxic drugs. On the other hand hyperthermia is a type of treatment in which body tissue is exposed to high temperatures to selectively damage and kill cancer cells. Although these diverse techniques are able to create cellular death but nonspecific cell binding can place healthy tissue in the surrounding at risk. Today it is a challenge to kill and control tumors at cellular level, using targets or markers that are able to identify and selectively attach to the tumor cells, allowing a more localised treatment. Thereby only the malign cells are killed and not the healthy tissues in the neighborhood and thus reduce harmful side effects. MNPs play a very important role in this modern cancer treatment.

2.1 In vivo Barriers

Human immune system has intrinsic biological barriers that help in the recognition and eventual destruction of foreign objects and serve to protect the body from harmful effects. Therefore, when therapeutics or contrast agents are injected in the body the first line of host defense keep them from reaching their intended destinations[20]. These barriers can restrict nanoparticle function by blocking their movement, causing physical changes to them, or by inducing specific biochemical signaling[21,22]. Upon intravascular administration nanoparticles immediately encounter blood plasma which has a highly ionic composition. In addition to coping with the vascular environment nanoparticles must overcome various anatomical size restrictions in the human body which limit their access to the target tissue. These size limitations are especially stringent when targeting certain organs like the brain and kidney[23]. For example, the blood–brain barrier (BBB) is a highly selective permeability barrier that separates the circulating blood from the brain extracellular fluid and it functions to hinder the delivery of diagnostic and therapeutic agents to the brain. To overcome the BBB the MNPs must be smaller than 10 nm – 20 nm[24].

2.2 Hydrodynamic Size

Within the vascular compartment nanoparticles encounter blood cells and plasma proteins and depending on their size and charge they may undergo adsorption or opsonisation by serum proteins. In addition to enhancing particle recognition by the host immune system, adsorption/opsonisation process alters the effective size of the nanoparticle and results in a particle diameter referred to as the *in vivo* hydrodynamic diameter, which may be considerably larger than the *in vitro* diameter

of the nanoparticle. The hydrodynamic size governs the nanoparticle concentration in the blood vessel, and their ability to extravasate from the blood vessel. While most endothelial barriers (interior surface of blood vessels) allow particles less than 150 nm in diameter to pass, as mentioned above the BBB is much more restrictive[24]. Hydrodynamic size also affects the mechanism of nanoparticle clearance from the human body.

2.3 Nanoparticle Clearance

Nanoparticles shows tremendous potential as multimodality agents with both imaging and therapeutic capabilities, however, only creating particles with optimal clearance characteristics will minimise any toxicity risks to the patient. The hydrodynamic size affects clearance from blood circulation and therefore blood half-life and also the whole body half-life. It has been reported that small nanoparticles (< 20 nm) are renally excreted[25] but medium sized nanoparticles (30 nm – 150 nm) accumulates in the bone marrow[26], heart, kidney and stomach[27], and large nanoparticles (150 nm – 300 nm) have been found in the liver and spleen[28]. While these size ranges provide general clearance criterion, other physical parameters also affects.

2.4 Surface Properties

Electric charge and hydrophobicity of nanoparticles can affect biodistribution by limiting or enhancing their interactions with the adaptive immune system, plasma proteins, extracellular matrices and non-targeted cells[29]. Specifically, hydrophobic and charged nanoparticles have short circulation times due to adsorption of plasma proteins (opsonisation) which can lead to triggering biochemical signalling and the host immune system may then remove the nanoparticles from circulation[30]. On the other hand, positively charged nanoparticles can bind with non-targeted cells (typically negatively charged) leading to nonspecific internalisation[16]. To limit interactions with the host, surface engineering of the nanoparticle is frequently adopted.

3. CORE-SHELL NANOPARTICLES

Widder[31], *et al.* first published their results of using magnetic albumin microspheres to target cytotoxic drugs (doxorubicin) in sarcoma (tumor) bearing rats. Since then the engineered biocompatible nanoparticle carriers have been considerably developed for imaging and for delivering drugs to specific target sites *in vivo* as well as for hyperthermia. Optimisation of these carriers continues today, however, generally the magnetic component of the particle is coated by a biocompatible material which can be functionalised. Silica is often considered as attractive coating for engineered nanoparticles, forming an inert and biocompatible outer shell. Not only does it create a protective shell against chemical degradation, it also allows surface functionalisation with, for example, functional alkoxysilanes[32]. These molecules then act as attachment points for the coupling of cytotoxic drugs or target antibodies to the carrier complex. A coated MNP with functionalised surface is schematically shown in Fig. 1.

Among the broad spectrum of nanoparticles being investigated for biomedical use, magnetic nanoparticles have gained much attention. This class of nanoparticle includes

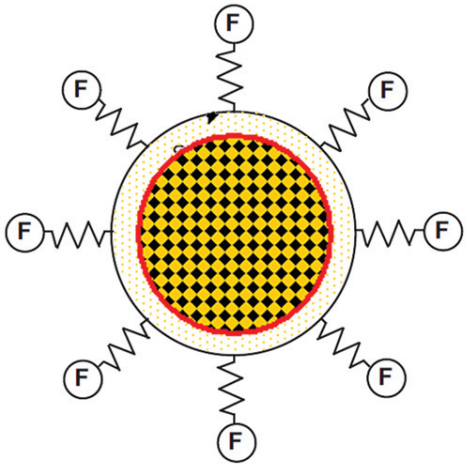

Figure 1. Schematic diagram of a functionalised core-shell MNP with a shell of silica (SiO_2) and function groups attached to the shell.

metallic, bimetallic, and superparamagnetic iron oxide nanoparticles (SPIONs)[32,33]. The use of colloidal iron oxide and iron oxide-based core-shell nanoparticles has attracted much attention for a wide range of applications[34,35]. Currently, several formulations of SPIONs have been developed as MRI contrast agents. A notable example being Feridex IV® (generic name for ferumoxide injectable solution) used for liver and spleen imaging and approved by the US food and drug administration (FDA) for human administration[36]. Another SPION formulation Combidex® for lymph node metastases imaging[36], although approved in some European countries did not succeed in gaining approval in the USA.

Despite their usage, SPIONs have several disadvantages, including rapid clearance by phagocytic cells (a cell, such as a white blood cell, that engulfs and absorbs foreign bodies in the bloodstream and tissues) and a limited trans-endothelia passage and tissue penetration[37]. There is therefore a need for the design of biocompatible MRI contrast agents with prolonged intravascular retention, improved tissue delineation, high chemical stability, and improved selectivity when targeting a tissue of interest. Other concepts such as biocompatibility or toxicity must be also taken into consideration. Further, in applications other than MRI contrast agents, e.g. hyperthermia, materials with higher saturation magnetisation are helpful. A number of alternative MNPs, ranging from metallic nanoparticles such as Fe, Co, Mn, Ni, Zn, Gd, Mg, and their oxides or intermetallics ($CoPt_3$, FePt, FeZn, Fe_3Al, etc.) have been investigated for their hyperthermic potential. Studies have demonstrated the biomedical potential of e.g. FePt and their core-shell alternatives, FePt-core/Fe_2O_3-shell and FePt-core/SiO_2-shell[12,38]. FePt has high Curie temperature, saturation magnetic moment, magneto-crystalline anisotropy, and chemical stability[38].

4. SYNTHESIS OF NANOPARTICLES BY ESPD

Electrochemical selective phase dissolution or ESPD was first developed in 2003 to produce nanoporous membranes from Ni-superalloys[14] and later adopted for nanoparticle synthesis[39]. For example, nanosised Ni_3Al-type intermetallic particles can be produce by extracting the intermetallic phase

from Ni-superalloys by selectively dissolving the matrix phase[13]. In principle, any metallic alloy containing two phases may be used as the starting material to produce nanoparticles. Essentially, the chemical composition of the alloy matrix must be different form the intended chemistry of the desired nanoparticle to be produced. Further, to produce nanoparticles of the intermetallic phase Ni_3Si for example, this phase must be present in the bulk alloy in a thermodynamically stable or a metastable state generally as precipitates or a second phase distribution. In systems where precipitates are coherently embedded in the alloy matrix (e.g. Ni–Al, Ni–Si, Fe–Al–Ni, Co-Al-W, etc), the morphology and size of precipitates are controlled to a large extent by the lattice-parameter misfit between the matrix and the precipitate phases. The nucleation and growth kinetics of such precipitates, especially aluminides and silicides, are well documented for different alloy systems[40]. Most of these precipitates can be controlled to ultra-fine sizes (in the nanometer range) by suitable heat treatments of the bulk alloys. Alternative to thermal treatments, processes like rapid quenching or severe plastic deformation can be used to produce nanosised second phase distribution in alloys. Essentially, ESPD is a two-step process: once the second phase is obtained as nanoscale dispersion, they can be separated from the bulk alloy by selective removal of the matrix by electro-chemical or chemical dissolution[41].

4.1 Electrolytic Phase Dissolution

The result of phase separation by ESPD is shown in Fig. 2. The microstructure of a typical Ni-base superalloy used in gas turbine application, after standard heat treatment, typically contain a bimodal distribution of γ' precipitates (Ni_3Al), regularly arranged in a γ matrix (Ni-Al solid solution). The microstructure of the heat treated bulk superalloys is as shown in the dark field transmission electron microscope (TEM) image in Fig. 2(a). The micrograph shows cuboidal γ' precipitates (~ 450 nm size) which are coherently embedded in the matrix and additionally smaller spherical secondary γ' precipitates (~ 70 nm in size) in the channels between the larger precipitates. Figure 2(b) shows a scanning electron microscope (SEM) image of the γ' precipitates (both the cuboidal and the secondary γ') after extraction by ESPD. The size correspondence between the precipitates/nanoparticles in Fig. 2(a) and 2(b) points to the clean extraction that is possible in the ESPD process[42].

A simple electrolytic cell maybe used for the selective removal of phase by electro-chemical dissolution in ESPD, where the alloy is used as the working electrode (anode) and platinum as cathode. In alloys containing two metallic phases (like in the Ni-base alloy shown in Fig. 2), the anodic polarisations of the two phases are different owing to their different chemical compositions. Essentially, for a given cell potential at which the two phases show different anodic current densities, the phase conducting higher current is preferentially dissolved. The cell potential, the current density, the composition of the electrolyte and its pH value are important process parameters in ESPD. These parameters can be experimentally determined from polarisation curves of individual phases, i.e. the current density as a function of the working electrode potential in a chosen electrolyte[13]. Polarisation curves from the matrix phase (Ni solid solution) and the precipitate phase (Ni_3Al) for the above example of Ni-base superalloy are as shown in Fig. 3. It is to be noted that pure Ni, instead of Ni-Al solid solution, is used as the reference material to approximate the matrix phase in this example. In Fig. 3, it is possible to find a range of potential values at which the two phases show considerable difference in anodic current densities (marked region in the figure). In the Ni-base alloys, both the precipitate and the matrix phases behave anodically because of their similar chemical composition (both contain Ni and Al); despite this, there is a significant difference in their dissolution rates. An aqueous electrolyte containing ammonium sulfate and citric acid (pH between 1.5 and 4) is suitable for the dissolution of the Ni-rich matrix phase in Ni-base alloys[39,43]. Selective phase dissolution maybe performed

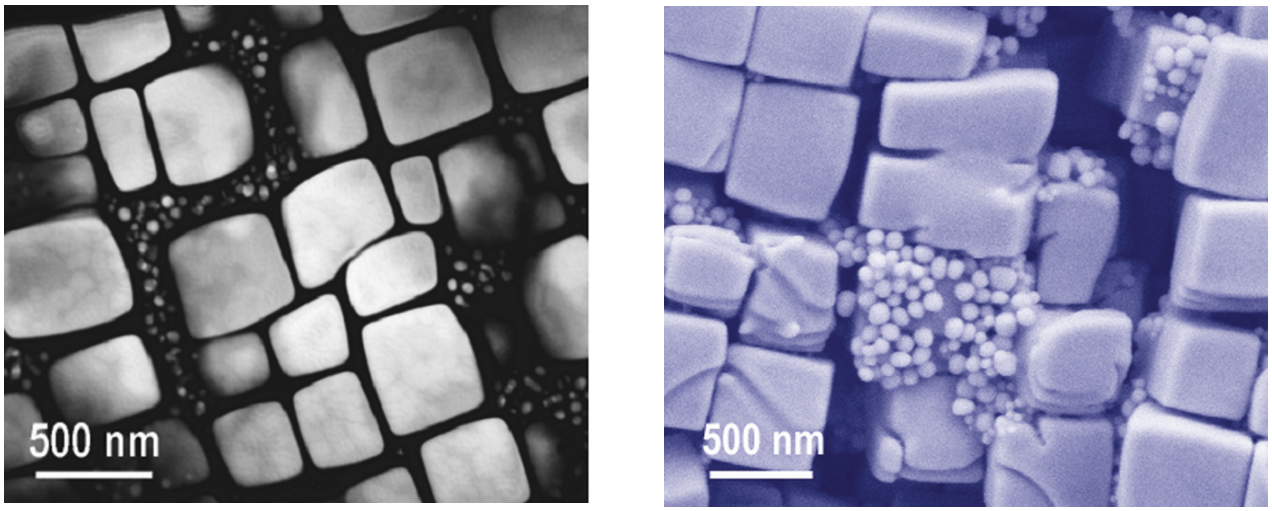

(a) **(b)**

Figure 2. Electron microscopic images of a typical two phase single crystal Ni-superalloy (a) TEM image showing bimodal distribution of Ni_3Al precipitate: large cuboidal shaped (~450 nm cube edge length) and small spherical shaped (~ 70 nm dia), which are embedded in a Ni-solid solution matrix and (b) SEM image of the precipitates after they are extracted from the alloy on dissolving the matrix by the ESPD process[42].

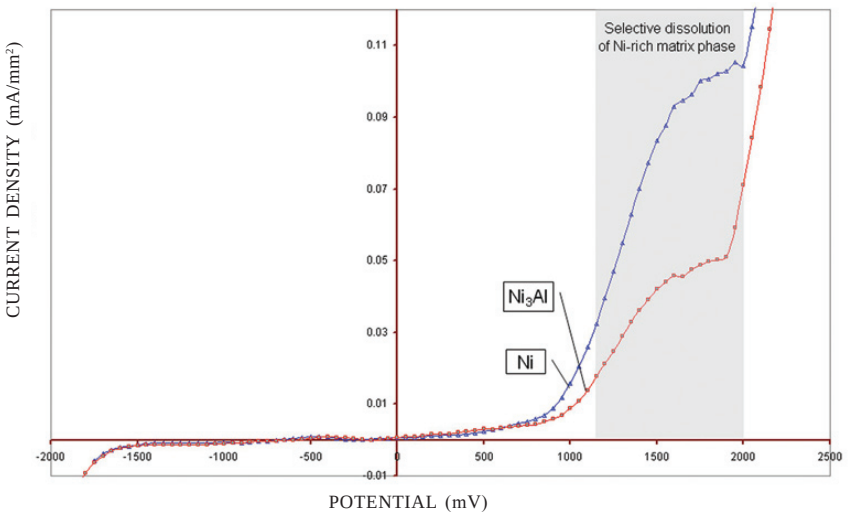

Figure 3. Anodic polarisation curves from the matrix (represented by Ni) and the precipitate (Ni_3Al) phases in Ni-superalloy showing a large difference in current density in the potential range marked in grey. Selective dissolution of matrix is possible in this range (electrolyte: aqueous solution of 1 % citric acid and 1 % ammonium sulfate with pH 2.4)[13].

electro-chemically at preselected current density (galvanostatic method) or at preselected potential (potentiostatic method). In other alloy systems where different atomic elements constitute the two phases, condition may exist where the matrix phase behave anodic (will dissolve) and the precipitate phase remains inactive/passive (cathodic). The reverse situation is also possible with suitable choice of electrolyte[14].

In this process of extraction of Ni_3Al precipitates (with ordered $L1_2$ crystal structure) from Ni–Al-base superalloys the nanoparticles developed no coatings, i.e. no shell formation was observed[39]. The ESPD process is however, very versatile and can be adopted also to produce core-shell nanoparticle. This is presented through Ni_3Si precipitates (also having $L1_2$ crystal structure) extraction from binary Ni–Si or ternary Ni–Al–Si alloys, where a core–shell nanoparticle with Ni_3Si or $Ni_3Si(Al)$ core with an amorphous SiO_x shell is produced[15].

TEM images of nanoparticles with and without a shell produced by ESPD are as shown in Fig. 4. The nanoparticle in Fig. 4(b) possesses a core–shell structure, which is formed during extraction in aqueous solution (acid). The shell uniformly covers the particle core.

4.2 Shell Formation Mechanism

The nanoparticles possessing the core–shell structure formed *in situ* during the extraction by ESPD. In order to understand how the shell may have been formed the relation between the composition of the two phases in the alloy from which the particles are extracted and their behaviour during electrochemical dissolution needs to be considered. The shell formation in the ESPD is a complex process where the electrochemical behaviour of the matrix and the precipitate phase in the bulk alloy are both involved. Broadly two processes are possible in anodic dissolution of a single phase (a solid solutions or a intermetallic phases) containing multiple atomic elements:

i. the phase may behave as a single entity like a pure metal and dissolve as a whole, or
ii. preferential leaching (de-alloying) of the less noble atoms in the phase may occur[44].

Whether a phase will be de-alloyed or dissolve like a pure metal depend mainly on two factors, i.e. the critical potential (which marks the onset of de-alloying) and the critical composition (the minimum concentration of the less noble element in the alloy which is necessary for de-alloying)[44]. The two critical parameters depend on the alloy and the electrolyte used. For alloys containing two phases, each individual phase has its own polarisation behaviour and therefore different types of reactions can be found to coexist in the same alloy. Generally, ordered intermetallic compounds having stronger atomic bonds have lower tendency for *de-alloying* than solid solutions[45].

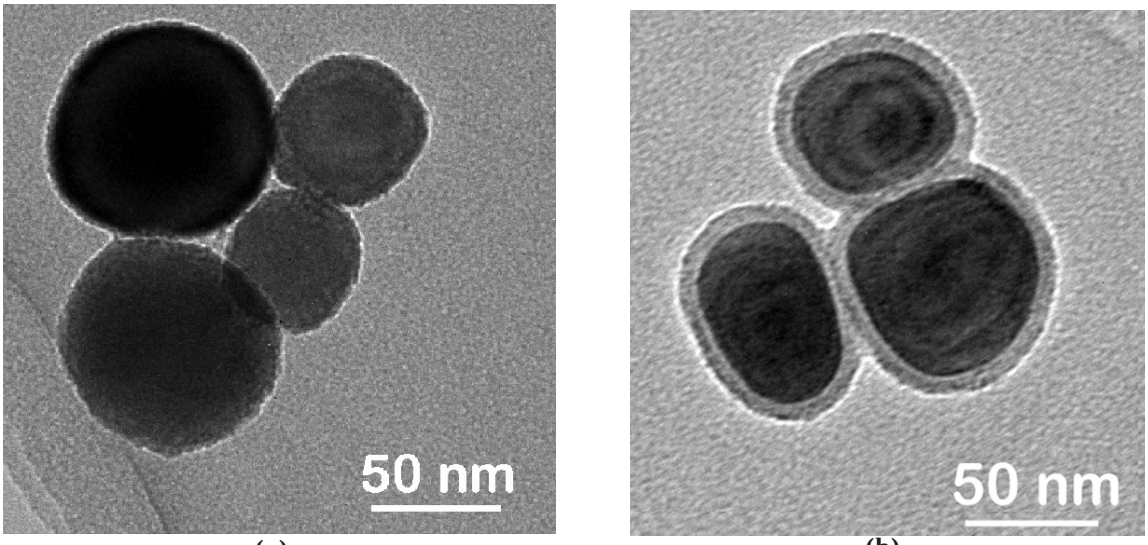

(a) **(b)**

Figure 4. TEM images of isolated Ni_3Si-type nanoparticles: (a) homogeneous particles, (b) particles having a core-shell structure[42].

To study how the shell is forming, the ESPD process was arrested in the middle of an extraction. That is to say, the process was interrupted when some of the nanoparticles were only partially extracted from the bulk alloy. In this state they remained partly embedded in the alloy surface. Cross-sectional specimens prepared from such partially etched anode allowed microstructural observation directly at the prior sample-electrolyte interface by TEM[46]. Figure 5 clearly shows that a shell has formed around the particle even before the particle is completely detached from the bulk alloy[47]. Further, it shows that the shell is of uniform thickness on the completely exposed particle surfaces, but becomes thinner near the region where the particle is still connected to the matrix. The particle shape and size is completely preserved, indicating that the matrix was only dissolved and the shell formed on top of the particle during the dissolution process.

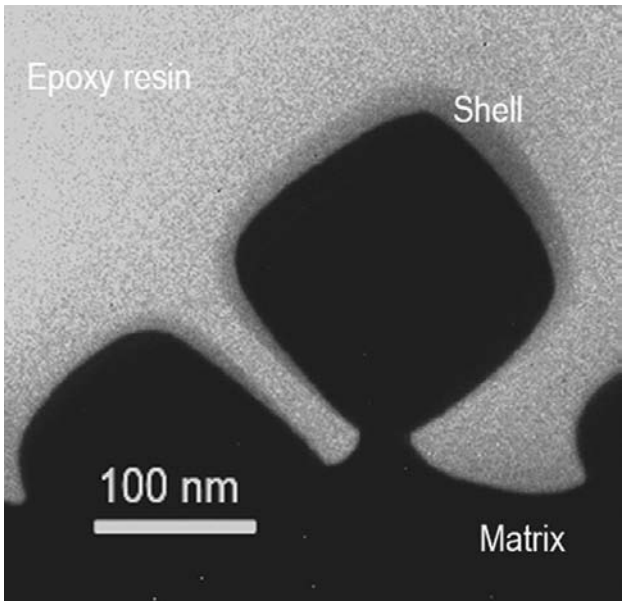

Figure 5. Cross-sectional TEM image of partially extracted nanoparticles show the shell formation in progress[47]. The shell is formed around the particle even before the particle is completely detached from the bulk alloy.

Shell formation was observed on Ni_3Si nanoparticles but not on Ni_3Al nanoparticles, both having ordered $L1_2$ crystal structures[42]. Moreover, the shell which formed is an amorphous Si-oxide. This suggests that the shell is produced by the oxidation of Si contained in the alloy and obtained by de-alloying of either the matrix or the precipitate phase during the extraction process. De-alloying of Si has been observed in Al-Si alloys, where Si behaves as the noble element[48]. Also in Ni-Al alloys de-alloying is reported but only in alloys with critical[44] Al concentration > 50 at per cent. There are mainly three possibilities (Fig. 6) for the shell formation by ESPD[15]:

i. Depletion of Ni from Ni_3Si precipitate and local diffusion of Si to the particle surface
ii. Depletion of Ni from Ni-Si solid solution matrix and local diffusion of Si on the particle surface
iii. Depletion of Ni from Ni-Si solid solution matrix and re-deposition Si as Si-oxide on the particle surface

Experimental observation of nanoparticle formation

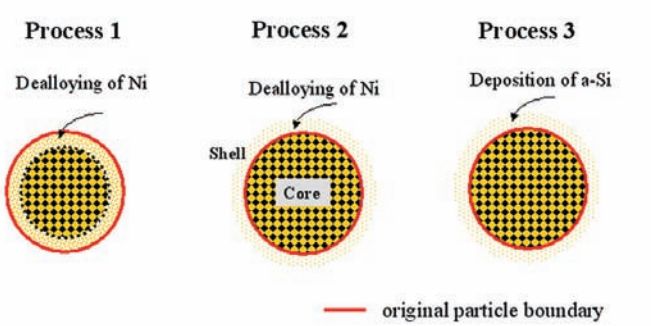

Figure 6. Schematic representation of three possible shell formation mechanism. In this example, the particle core is Ni_3Si intermetallic phase and the shell is an amorphous Si(O) phase[47].

(Fig. 5) as well as, their shape and size after extraction clearly show that the Ni_3Si precipitates are not attacked by electro-corrosion[47]. Therefore, the first model can be excluded. The other two models consider de-alloying of the alloy matrix to obtain free Si, and differ only in details of how the Si is redistributed on the particle surface. Later of these two models appear to be the likely mechanism of shell formation in ESPD. Thus Ni preferentially dissolves from the solid solution matrix and the Si acts as a noble metal, like in the Al-Si and is left undissolved. The free Si is oxidised in the aqueous electrolyte solution and deposit on the freshly exposed surface of the extracted precipitates[15].

4.3 Collection of Extracted Nanoparticle after ESPD

The nanoparticles extracted by ESPD (with or without shell) get dispersed in the electrolyte or stick to the anode (sample) surface. Small particles (< 100 nm) have strong surface adhesion tendency and stick to the electrode surface after extraction, even after completely freed from the bulk alloy. They are collected from the anode by ultrasonic cleaning in alcohol and not from the electrolyte solution. So some nanoparticles are lost in the electrolytic solution, but this loss is very minimal. As the tiny particles in the electrolyte solution remain in suspension for long duration and do not settle down in reasonable time, separating them from the liquid by gravity is not easy. Separation by filtering is also not effective because filters with sub micrometer pores are expensive. Further, the particles readily choke the filter and collecting them from the filter is not efficient. The most effective way is to collect the particles from the anode by ultrasonically dislodging them from the surface in a methanol bath. The electrolytic extraction process is interrupted and the anode transferred to the ultrasonic bath at regular intervals. This process can be automated. The nanoparticles remain in suspension in the alcohol and are finally collected by centrifuging. Powder samples can be kept stored in alcohol in a capsule until needed, before centrifuging and drying. This way contamination can be minimised.

4.4 Contamination of Nanoparticles

A critical issue in nanoparticle collection is contamination by the electrolyte. Nickel ammonium sulphate has been revealed by X-ray diffraction (XRD) and energy dispersive

spectroscopy (EDS) measurements in some samples of nanoparticles collected directly from the electrolyte. This is a salt which forms in the electrolyte due to the presence of Ni^{++}, ammonia and sulphate ions[46]. However, as this salt is soluble in water, the contamination can be easily removed by repeatedly washing the powder in de-ionised water.

5. CHARACTERISTICS OF NANOPARTICLES SYNTHESISED BY ESPD

The various nanoparticles produced by ESPD were extensively characterised using neutron and X-ray diffraction, electron microscopy (TEM/SEM) and *in situ* small angle neutron scattering (SANS) to determine their structure, composition and properties. This included also the core-shell nanoparticles. The results have been published[13,15,39,42,47] and here important characteristics mainly for the Ni_3Al and Ni_3Si nanoparticles are presented. Successful extraction has been recently carried out in other systems (e.g. Ni-Fe-Si or Co-Al-W) for example also to obtain Ni_3Fe and $Co_3(Al,W)$ MNPs with core-shell structure[49].

In the ESPD process described above, it is generally possible to control the nanoparticle size in a wide range (from a few nm to submicron sizes) but the particles can also be produced in a narrow size band. The shape, size and composition of the particles are determined in the solid state in the bulk alloy where the second phase is generally in a stable thermodynamic state and therefore, even the multi-component intermetallic phase nanoparticles synthesised by ESPD are chemically homogeneous. It may be pointed out that complex nanoparticles with homogeneous composition are not easy to produce by many of the other processes of nanoparticle synthesis, e.g. physical or chemical vapor deposition, hydrogen plasma reaction, mechanical alloying or electrodeposition. The ESPD process can produce nanoparticles which are clean, homogeneous, monocrystalline, and defect or stress free. It can also be tailored to produce nanoparticles with a core-shell structure. Monocrystalline and defect-free core-shell MNPs are particularly interesting for biomedical applications for their single domain magnetic structure. Amongst these Co-based MNPs show special attraction, with intermetallics and amorphous nanoparticles based on Co-W, Co-Al, Co-Pt, and Co-Ir systems being notable[50].

5.1 Structure and Composition of Intermetallic Nanoparticles

Intermetallic compounds are made of two or more metals or of a metal and a nonmetal. Metallic aluminides and silicides are examples. Intermetallic bulk materials offer properties useful in many applications for their low density, good electrical and heat conductivity and in some case, they are magnetic. Transition metal aluminides and silicides based on iron, cobalt and nickel constitute an important class of intermetallic compound for technological applications. The metal-rich nickel silicide Ni_3Si, for example, has been identified as a promising candidate for several applications (high temperature energy conversion equipment or as gate in nano-electronics devices)[51,52]. According to the binary Ni–Si phase diagram[53], β_1 Ni_3Si has no congruent melting point and is formed by solid-state (eutectoid and peritectoid) reactions of monoclinic β_2 Ni_3Si or hexagonal γ Ni_5Si_2 phases[54]. Synthesis of Ni_3Si nanostructures is therefore not straightforward but different routes are available for their synthesis. For example, synthesis of freestanding Ni_3Si nanowires by high temperature chemical reaction in gas phase has been reported[55], also there were attempts to produce nanoparticles of Ni_3Si by elemental blending of Ni and Si powders through mechanical alloying[56]. In a recent publication we demonstrated that nanoparticles of Ni_3Si can be produced by ESPD[15] and they can have a core-shell structure[57].

A high-resolution electron microscopy image of a single nanoparticle of Ni_3Si is shown in Fig. 7. By precisely orienting the particle in the electron beam with the help of a double tilt goniometer stage in TEM a lattice-resolved image of the nanoparticle could be obtained[42]. The single isolated Ni_3Si nanoparticle (~20 nm diameter) is oriented with the [001] direction parallel to the electron beam in Fig. 7(a). The selected area diffraction image from the particle (Fig. 7(b)) shows that it is a single crystal with a high degree of ordering. The lattice is defect free and extends right up to the surface atomic layer in the particle. It further shows that the structure is very uniform

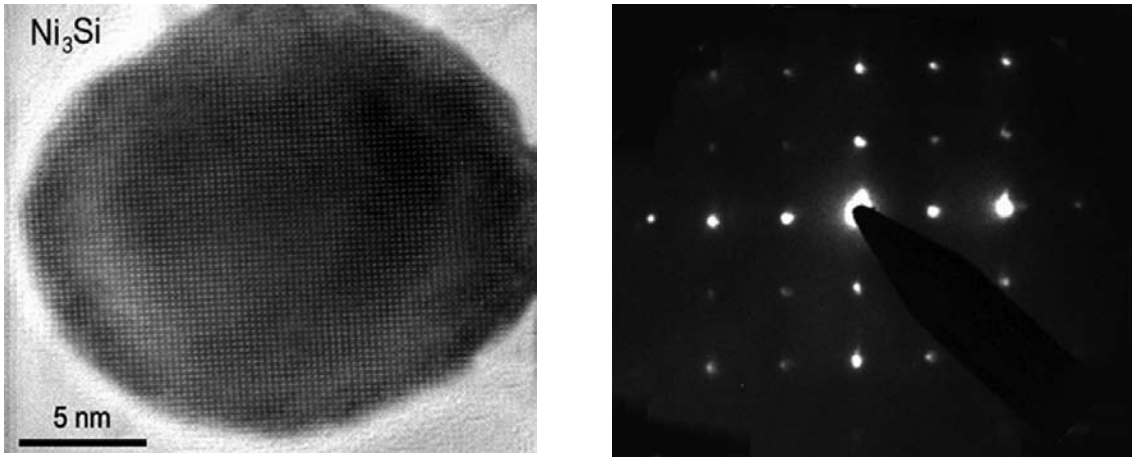

(a) **(b)**

Figure 7. (a) A lattice-resolved HREM image of an isolated Ni_3Si nanoparticle (~20 nm diameter) oriented in [001] direction, (b) selected area electron diffraction pattern shows that the nanoparticle has an ordered $L1_2$ crystal structure[42].

and there is no distortion in the lattice, even near the free surface. Figure 8(a) shows a high resolution image of a typical $Ni_3Si(Al)$ type core-shell nanoparticle[42]. The magnified image in Fig. 8(b) shows that the particle core and the shell have completely different structures. The core, where the atomic columns of the $L1_2$ lattice are resolved, is crystalline (here oriented along the [110] beam direction). The interface between the core and the shell is very sharp, within a few Å, and the outer boundary of the shell is also very smooth. The shell is clearly not crystalline and shows a contrast typical of an amorphous phase. Both the Ni_3Si-type nanoparticles shown in Figs. 7 and 8 were produced by ESPD. Nanoparticles with sizes ranging from less than 20 nm to more than 150 nm and a uniform shell thickness of 3 nm - 20 nm can be easily produced by ESPD.

The crystallographic structure of the core and the shell of the nanoparticles were investigated by electron powder diffraction and also by neutron and X-ray diffraction[42,57]. There are a few critical aspects which influence the quality of the Debye-Scherrer ring pattern (Fig. 9(a)) and the resolution of the powder profile analysis. First of all, a precise centering of the ring pattern is important for a proper azimuthal averaging of intensities in the ring pattern. For analysis, we used a graphical aid in the form of a help circle, as a guide for centering. The bright Debye-Scherrer rings in the pattern were matched with the guide circle, whose center then provided the pattern center. For precise measurement of lattice parameters the camera length of the microscope was also calibrated with standard gold powder (a_{Au} = 0.40786 nm). The measured powder

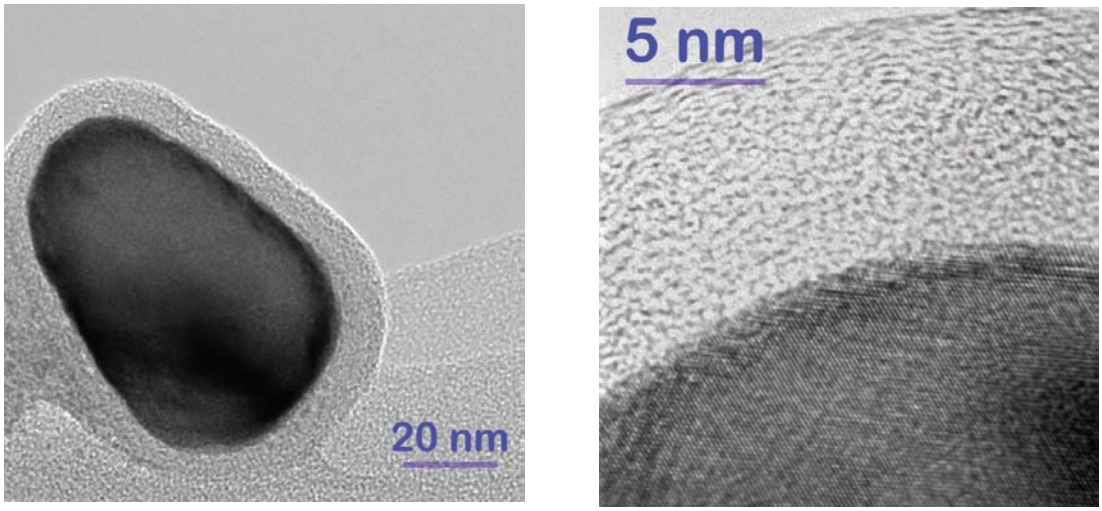

(a) **(b)**

Figure 8. (a) A HREM image of an isolated $Ni_3Si(Al)$ nanoparticle (~ 80 nm diameter) with a core-shell structure. (b) A higher magnification image from part of the particle. The crystalline core of the particle is imaged in the [110] beam direction and the shell has an amorphous structure[42].

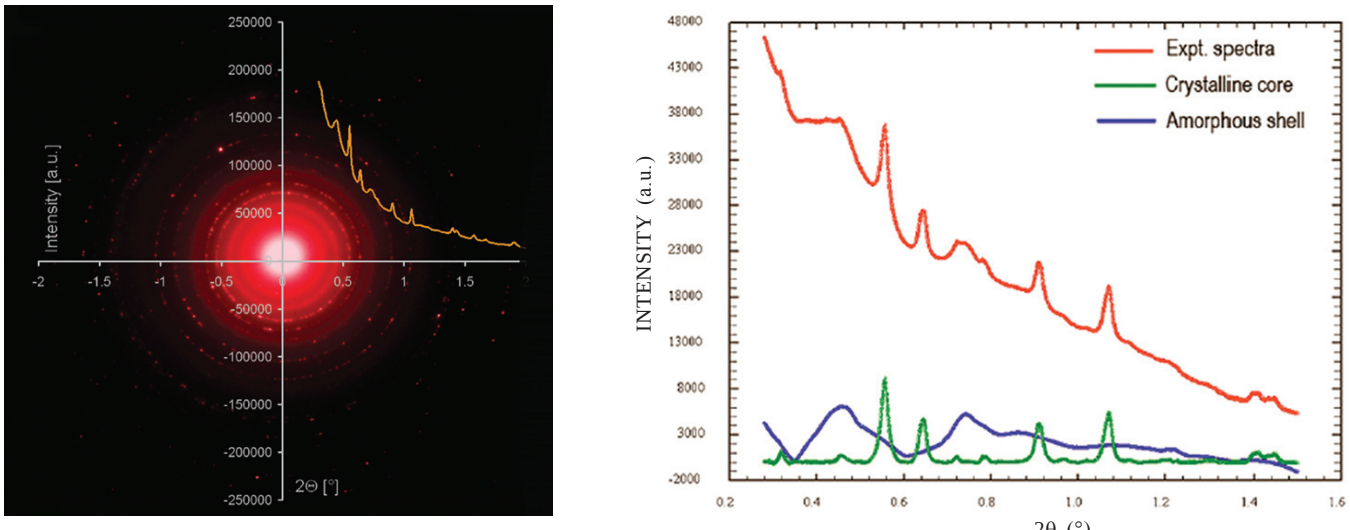

(a) **(b)**

Figure 9. Electron diffraction from core-shell $Ni_3Si(Al)$ nanoparticle powder: (a) Debye-Scherrer ring pattern and the superimposed diffraction pattern, (b) Intensity *vs*. scattering angle profile obtained from azimuthally averaging intensities in Debye-Scherrer rings. (red curve). This is a summation of two spectra: (i) sharp peaks (green curve) from $L1_2$ structure of the crystalline core and (ii) broad diffuse peaks (blue curve) from the amorphous shell around the nanoparticles[42].

diffraction patterns were analysed using the FullProf software[58] applying the Rietveld refinement technique[59]. The presence of crystalline core and amorphous shell is revealed in the powder electron diffraction pattern (Fig. 9). The measured spectrum (red curve in Fig. 9(b)) is a superposition of contributions from two different structures:

(i) The sharp peaks (green curve) matching the $L1_2$ structure of the crystalline core of the $Ni_3Si(Al)$ nanoparticles; and

(ii) The broad diffuse peaks (blue curve) corresponding to a modulated intensity due to coherent scattering from an amorphous phase, is attributed to the particle shell.

The positions of the broad peaks, determined from the electron powder diffraction data, are listed in Table 1 and compared to the XRD results (from the same powder sample)[15]. The first broad peak at Q = 1.7 $Å^{-1}$ seen in the XRD pattern, is, however, not observed in the electron diffraction pattern because at very low angles the electron powder pattern is strongly affected by the very high background resulting from the tail of the primary transmitted beam. The lattice parameter of the $N_3Si(Al)$ particle core determined by electron (0.3513(3) nm) and X-ray diffraction (0.35094(3) nm) agree very well. This attests to the quality of the electron diffraction measurement and the data analysis method adapted.

The composition of the core and the shell was measured by energy dispersive X-ray spectroscopy in TEM[42]. Typical EDS results are shown in Fig. 10(a). In Fig. 10(b), the bright field TEM image of a single core-shell nanoparticle of $Ni_3Si(Al)$ with three contamination marks (one in the core and two in the shell region) is seen. These marks indicate the actual position where the beam was focused on the specimen to obtain the EDS spectra. Measurement from the narrow shell (~15 nm thick) is possible. However, as the particle core is covered by shell all around, measurement in the core region always included a small volume of the shell material. This contribution from the shell could not be separately estimated and is ignored considering that the involved shell volume is extremely small. All the measured spectra show presence of Cu and C peaks, since the powder was placed on a carbon foil on top of a copper grid. Therefore, Cu and C are ignored in the quantitative evaluation of the core and the shell compositions. The EDS spectrum from the core (blue) of $Ni_3Si(Al)$ nanoparticles shows the presence of O, Ni, Si and Al, while that from the shell (red) contains only Si and O peaks (Fig. 10(a)). The shell thickness is narrow, so there is always the possibility that the beam may touch the core during a measurement in the shell. However, this is easily detected after the measurement from the contamination spots (e.g. see the contamination spot marked by golden yellow dotted circle in Fig.10(b)) and the corresponding spectra (golden yellow colour curve in Fig. 10(a)) where the Ni peak is readily detected. Such unsuccessful measurements are rejected. The absence of Ni and Al in the shell is an indication that the oxide shell forms upon de-alloying of the Ni-Si-Al

Table 1. Diffraction results from measurement on core-shell Ni_3Si nanoparticles synthesised by ESPD. The broad peak positions from the amorphous shells obtained by electron and X-ray powder diffraction are compared[42].

Peak position 2θ (°)	Scattering wave vector Q ($Å^{-1}$)
Electron powder diffraction	
0.43	2.4
0.72	4.0
0.85	4.7
X-ray powder diffraction	
24.0	1.7
34.5	2.4
60.5	4.1
72.0	4.8

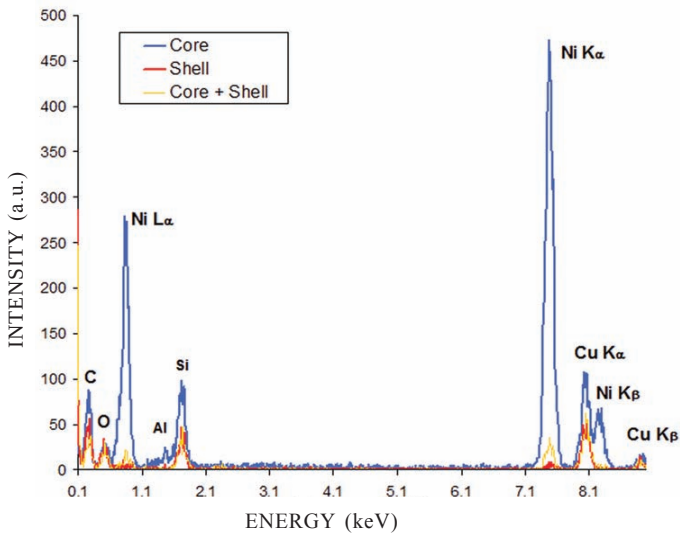

(a)

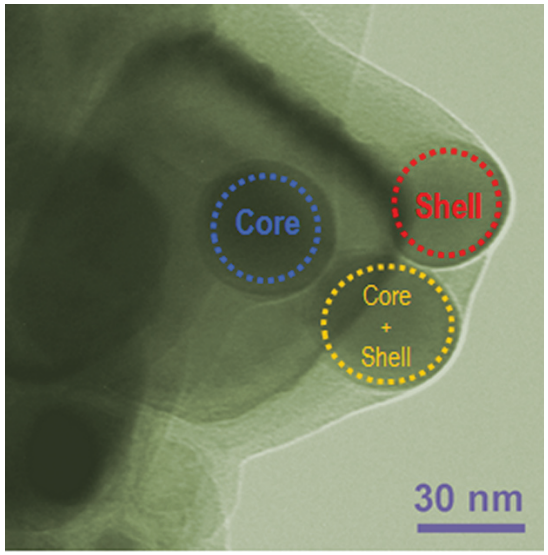

(b)

Figure 10. Core and shell compositions of nanoparticles measured using energy-dispersive X-ray spectroscopy in the TEM. Typical EDS spectra from core and shell region, (b) bright field TEM image of the core-shell nanoparticle showing three contamination marks (one in the core and two in the shell region) where the beam was focused for the EDS measurements[42].

matrix solid solution which preferentially dissolve Ni and Al. Oxygen peaks are detected in the spectra from both core and shell; but it is not priori clear if oxygen is actually present in the core also. Considering the discussions above, it is concluded that oxygen is present only in the shell and Ni, Al, and Si are the only elements in the particle core; same as in the precipitates in the bulk alloy. The results shows that the shell of the $Ni_3Si(Al)$ nanoparticles contain 85 % O and 15 % Si and its core contains 67.7 % Ni, 29 % Si, and 3.3 % Al (in at. %). The measured Si content is higher than in Ni_3Si β1 phase (22.5 to 24.5 at. % Si)[53]. The excess Si is partly a contribution from the shell volume measured along with the core.

Details of structure and composition at interfaces can be obtained by small-angle neutron scattering (SANS) using contrast variation method[60]. This technique was used to characterize core-shell nanoparticles produced by ESPD[61]. The distinctly different neutron scattering lengths of hydrogen and deuterium is exploited in the SANS contrast variation experiment to reveal details of structure and compositions at the interfaces[62]. An example is presented from the measurement of core-shell Ni_3Si nanoparticles. Figure 11 displays the measured SANS data of nanoparticles dispersed in the H_2O/D_2O mixtures having different concentrations. By changing concentration of the mixture a condition is obtained when the scattering contrast of the mixture equals that from the shell of the nanoparticle, so that the shell become invisible and only scattering from the particle core is detected. Scattering length density (SLD) of the shell is determined from this measurement to be about 49.7×10^9 cm^{-2}. The SLD of crystalline SiO_2 (mass density 2.60 g/cm^3) is much less, i.e. 41.0×10^9 cm^{-2}. TEM measurements showed that the shell is amorphous SiO_x with 85 % oxygen, which is higher than in stoichiometric SiO_2. The higher oxygen content will increase the SLD (48.8×10^9 cm^{-2}), however, a lower mass density (2.20 g/cm^3) can be expected for the amorphous shell. Therefore even after taking into account the high oxygen amount, the SLD value of the amorphous

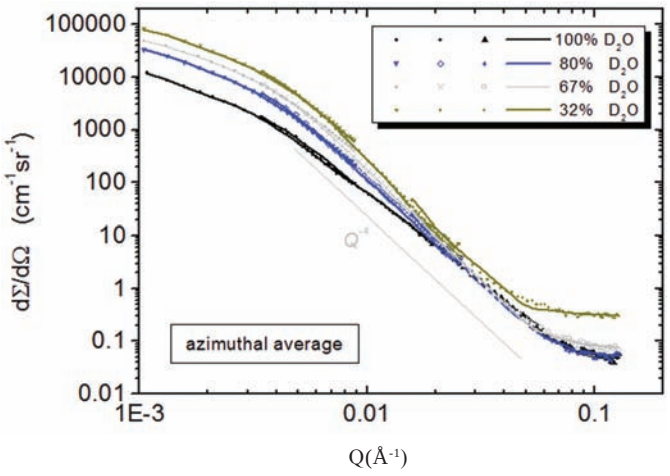

Figure 11. Neutron scattering from Ni_3Si core-shell nanoparticle powder dispersed in a mixture of H_2O/D_2O solutions with different concentration of D_2O (and therefore different SLD). To cover a wide Q range each measurement was made at wavelengths of 1.96 nm, 1.03 nm and 0.637 nm[61].

shell is low (41.2×10^9 cm^{-2})[13]. This discrepancy in SLD can be resolved if one consider that OH^-/H^+ ions are present in the shell. As hydrogen and hydroxyl ions are abundant in the electrolyte used in ESPD synthesis and considering the shell formation mechanism described above, their presence in the shell of the nanoparticle is quite likely.

5.2 Nanoparticle Size and Size Distribution

Nanoparticles synthesised by ESPD can be tailored to produce particles with a wide size range but most MNPs are desired in rather small sizes (~ 10 nm – 20 nm) and in narrow size distribution. SANS is a powerful tool for the measurement of powder particles, as well as, inhomogeneities less than 100 nm size in bulk solid and is particular effective for the measurement of sizes close to a nanometer. The core–shell nanoparticles produced by ESPD were characterised by SANS and their particle size distribution (PSD) determined. Figure 12 shows the azimuthally averaged neutron scattering intensity of Ni_3Si nanoparticles dispersed in H_2O and D_2O and the calculated particle size distribution (core + shell), determined from the fitting of the neutron intensity profile. The powder sample designated Ni_3Si-2 has a unimodal distribution of core-shell nanoparticles with average particle size (20 nm, core + shell) and a narrower size distribution (Fig. 12(b))[62]. It is possible to synthesised nanoparticle with a different PSD (e.g. bimodal with average particle size of 93 nm and 215 nm for the smaller and larger populations, respectively) from the same alloy, by differently heat treating the alloy before extracting the particle by ESPD[61,62]. This demonstrates the versatility of the ESPD method.

Shell thickness of the two samples of nanoparticles (Ni_3Si-1 and Ni_3Si-2) is also determined from the SANS experiment. They have different shell thicknesses: the bimodal Ni_3Si-1 having an average shell thickness of 17 nm for the larger and 5 nm for the smaller size population, respectively[61]. The smaller size Ni_3Si-2 nanoparticles have even thinner shell, only 3 nm thick[62]. It is apparent that the shell thickness scales with the particle size. This size effect can be explained by considering the anodic polarisation to which the precursor alloy is subjected during precipitate extraction in the ESPD synthesis process[15]. During the ESPD process, the time a precipitate particle remains attached to the precursor alloy is proportional to its size. A thicker oxide shell can therefore form around larger particles as they keep an electric contact with the precursor alloys for a longer time. That the scaling effect is found for nanoparticles of different dimensions in the same alloy exclude the possibility that it is solely an oxidation effect in the electrolytic solution. The size effect is also observed in extraction of nanoparticles from different alloys[62]. However, the extraction process parameters (particularly the pH value of the electrolyte) may be varied in order to build up shells with different thickness.

5.3 Magnetic Properties of Nanoparticle Synthesised by ESPD

First measurements of magnetic properties on nanoparticles synthesised by ESPD were reported on Ni_3Al particles[39]. Measurements were done on two samples both of

which contained relatively large particles: Sample-I having 450 nm nanoparticles with a relatively broad PSD and Sample-II with ~ 90 nm nanoparticles. The temperature dependence of the magnetisation of powders of Sample I and Sample-II are as shown in Fig. 13(a), while the measured hysteresis loops at different temperatures from the smaller particles (Sample-II) are as shown in Fig. 13(b). Stoichiometric Ni_3Al in macro/bulk size is reported to have a Curie point of 40 K and is one of the most extensively studied weak itinerant ferromagnet[63]. The early experiments in ESPD used multicomponent Ni-superalloys as the bulk alloy (with Ta, W, Mo, and Cr addition) from which the Ni_3Al nanoparticles were extracted[39]. These are not intended for MNP applications but the experiment demonstrated the suitability of ESPD for nanoparticle synthesis. This is a novel process for nanoparticle synthesis with some unequalled advantages as discussed above.

ESPD was next applied to produce nanoparticles of Ni_3Si phase, whereby production of core-shell nanoparticle is demonstrated. While many investigations on electronic properties of Ni_3Si nanostructures are found in the literature[51,52], magnetic properties of Ni_3Si have drawn less attention. Some nickel silicides (Ni_2Si, NiSi, and $NiSi_2$) are ferromagnetic at room temperature[64], however, the non-continuous changes of electronic density of Ni silicides with Si do not allow the behaviour of Ni_3Si to be inferred from the other intermetallics of Ni-Si. Only a few reports on magnetic properties of bulk Ni_3Si are found in literature, which essentially discusses Ni_3Si in the context of Ni_3Fe[65,66]. It is demonstrated that Ni_3Si nanoparticles produced by ESPD are superparamagnetic at low temperatures, when they are in sizes below 200 nm[63].

The magnetisation curves of the Ni_3Si-2 (20 nm, core + shell) nanoparticles, field cooled (FC) in an applied magnetic field and zero field cooled (ZFC) between 3 K and 40 K are shown in Fig. 14(a). The ZFC curve separates from the FC curve at 11

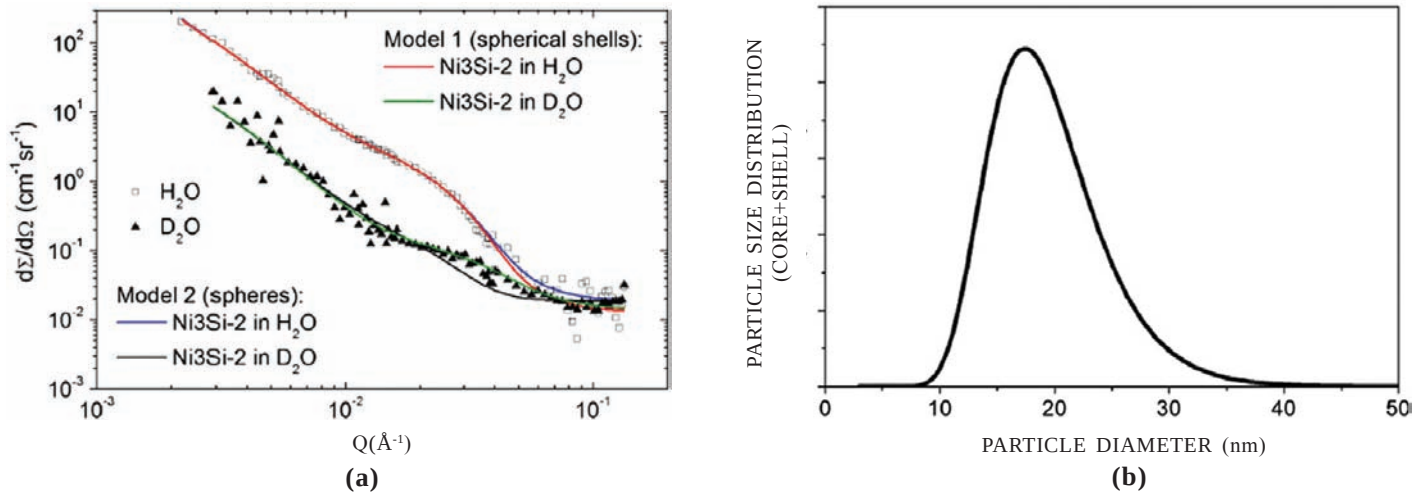

Figure 12. Small angle neutron scattering from Ni_3Si nanoparticle powder dispersed in H_2O or D_2O solutions: (a) The symbols represent azimuthally averaged neutron scattering data points from the Ni_3Si-2 sample. Fits based on two models: one representing incoherent scattering from a distribution of spherical shells (Model 1) and the other scattering from a distribution of spherical core (Model 2) are added (solid lines) and (b) Calculated particle size distribution (core + shell) calculated from fitting of SANS data according to the core-shell models[62].

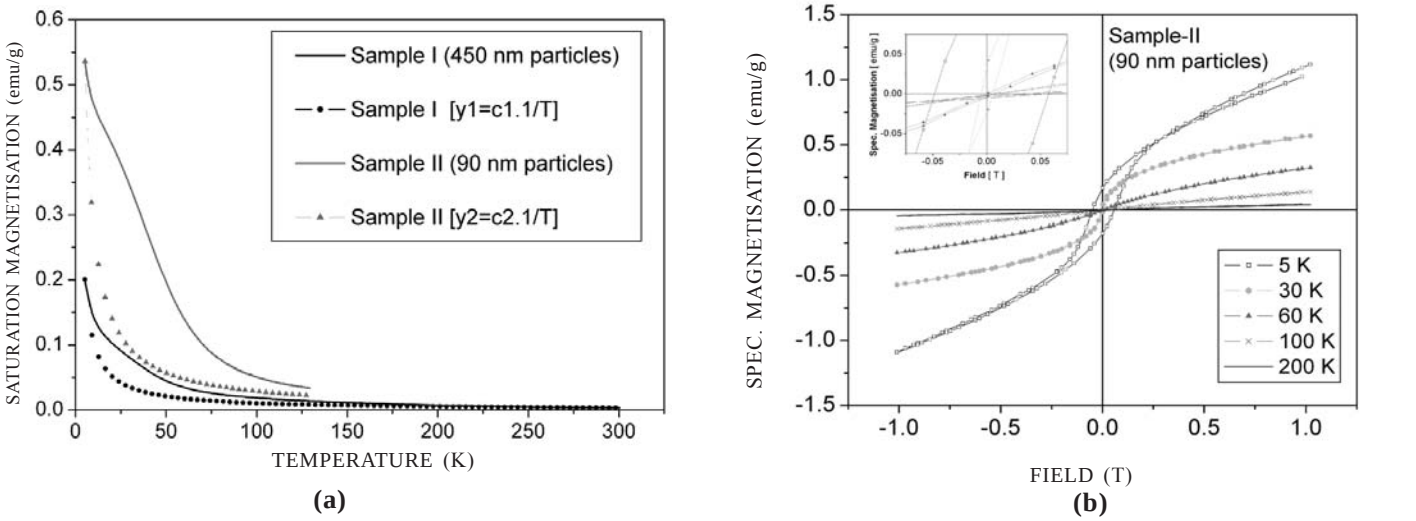

Figure 13. (a) The temperature dependence of the specific magnetisation of the two Ni_3Al nanoparticle samples I (size 450 nm) and II (size 90 nm) and (b) Hysteresis loops from sample II[39].

K which corresponds to the blocking temperature (T_B) for the Ni_3Si-2 nanoparticles. The corresponding field-dependent magnetisation curves recorded at different temperatures between 5 K and 150 K are shown in Fig.14(b). It is known that when a bulk ferromagnetic material is reduced to nano-size, single-domain magnetism dominates and the magnetic property of the material is changed. The extracted nanoparticles (β_1-Ni_3Si phase) exhibit a paramagnetic to ferromagnetic transition with low coercivity and saturation magnetisation (> 20 emu/g) at low temperatures (< 11 K) and this is interpreted as superparamagnetic behaviour of single domain nanoparticles[62]. Magnetic exchange interaction between silica shell and magnetic core is not expected, but the non-magnetic silica shell partially suppresses the overall magnetic signal of the nanoparticles. However, it does not change the magnetic character of the core and only reduces the overall magnetisation that could be measured. A silica shell surrounding the nanoparticles can be an advantage for applications as it can protect from environmental degradation and also provide attachment sites for polymers, in case functionalisation of particles surface is required for achieving stable colloidal suspensions and medical use.

6. VERSATILITY OF ESPD PROCESS

Electrolytic processes in general have been used to produce different nano-structured materials, in particular de-alloying of homogeneous alloys for the fabrication of nanoporous structures (e.g. nanoporous gold)[67], the fabrication of alumina nano-templates prepared by galvanostatic anodisation[68], and electrodeposition techniques which are used to produce nanowires[69], for example, to name a few. The ESPD process described here is not only useful for synthesising nanoparticles but can also be adopted to produce a multitude of different nanostructures.

Selective phase dissolution is an important processing step in ESPD for the fabrication of nanoparticle. ESPD is however a *two-step* process. In the *first step* of nanoparticle synthesis, nano sized second phase precipitate distribution is created in the bulk alloy and then in the *second step* the matrix phase is dissolved, leaving a powder of isolated nanoparticles. The electrolytic process is selective and actually either the matrix or the precipitate can be dissolved[13].

So in the *second step*, if instead of dissolving the matrix the precipitates are dissolved (being not connected they will be dissolved only on the surface) a nanostructured template is created on the surface of the bulk alloy. For a regular array of precipitates, this structured surface can have special characteristic, which is in itself tunable. This for example can be tailored to fabricate a template for tissue engineering. On the other hand, if in the *first step* the alloy is so treated that the second phase structure is interconnected and in the second step this interconnected phase is dissolved as nanoporous structure can be created[13]. This is similar to nanoporous gold produced by de-alloying[67], but the pore structure being channel-like and in regular array with tunable pore size[43]. The different variations of the ESPD process is schematically depicted in Fig. 15. More details about the ESPD process and its variations can be found in literature[13,43].

One of the advantages of ESPD over other nanoparticle synthesis methods is that it can, not only produce very small nanoparticles in a narrow size band, it is equally suitable to produce rather large nanoparticles (up to 500 nm size) with complex structure, composition and shape. The large nanoparticles may not be so much attractive for their special physical or chemical properties, but being defect and stress free intermetallic monocrystalline, they does have attractive structural and mechanical properties[71]. Such large submicron particles with homogenous structure and composition are very difficult to produce through so called bottom up nanostructure fabrication processes. Cubic shaped intermetallic Ni_3Al particles for example, were envisaged in the fabrication of nano sized components for micron/submicron sized robots by nano-forging route[71].

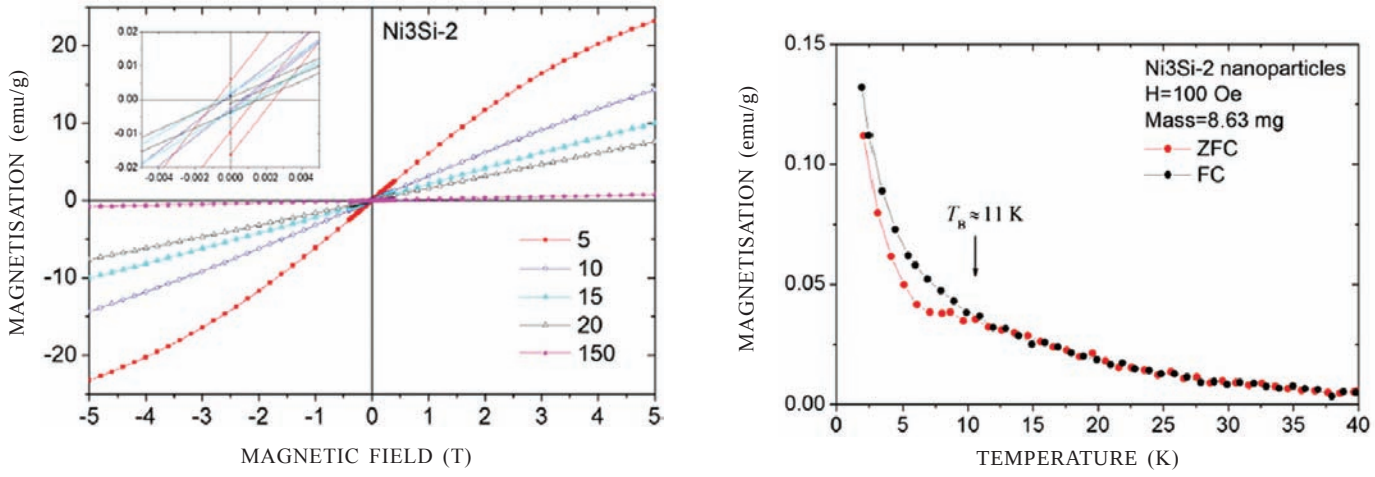

Figure 14. Magnetic property of Ni_3Si nanoparticle synthesised by ESPD: (a) FC and ZFC curves of the powder sample Ni_3Si-2 (size 20 nm) at 100 Oe, and (b) corresponding M(H) curves recorded at different temperatures between 5 K and 150 K.

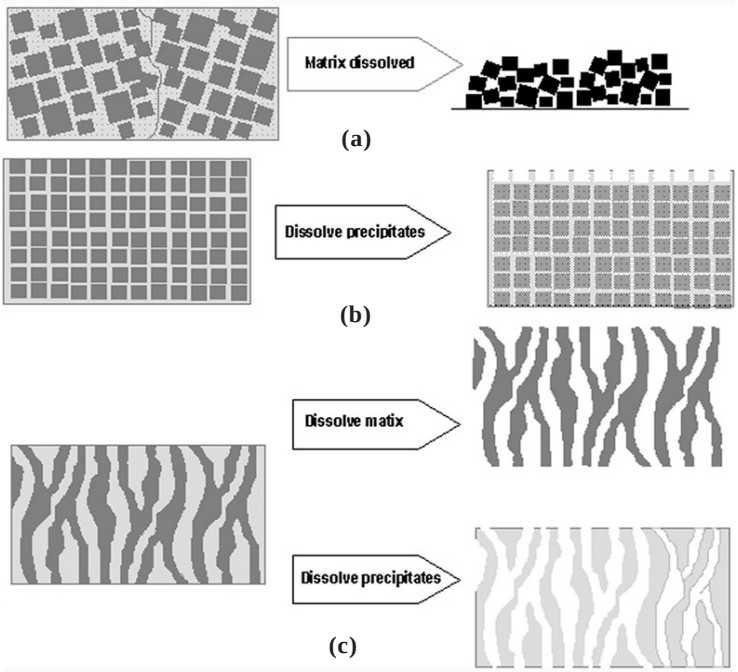

Figure 15. Versatility of the ESPD process: (a) when the matrix is dissolved in a polycrystalline alloy with nano-sized precipitates, nano-particles are obtained, (b) when precipitates at the surface are dissolved in an oriented single-crystalline alloy with regularly arranged nano-sized precipitates, a nano-template is obtained, and (c) when the matrix or the precipitate phase is dissolved in an alloy with interconnected precipitates (e.g. rafted microstructure in Ni-superalloys), a nano-porous membrane is obtained[15].

REFERENCES

1. Gleiter, H. Nanocrystalline materials. *Progress Mat. Sci*., 1989, **33**, 223–315. doi: 10.1016/0079-6425(89)90001-7
2. Binns, C. Nanoclusters deposited on surfaces. *Surface Sci. Reports*, 2001, **44,** 1–49. doi: 10.1016/S0167-5729(01)00015-2
3. Sanvicens, N. & Marco, M.P. Multifunctional nanoparticles-properties and prospects for their use in human medicine. *Trends Biotechnology*, 2008, **26,** 425–433. doi: 10.1016/j.tibtech.2008.04.005
4. Pankhurst, Q.A.; Connolly, J.; Jones, S.K. & Dobson, J. Applications of magnetic nanoparticles in biomedicine. *J. Physics D: Appl. Physics*, 2003, **36**, R167–R181. doi: 10.1088/0022-3727/36/13/201
5. Mulvaney, P. Metal Nanoparticles: Double Layers, Optical Properties, and Electrochemistry. *In* Nanoscale Materials in Chemistry, K.J. Klabunde (ed), New York, John Wiley & Sons, Inc. 2001, pp. 121–168.
6. Schärtl, W. Crosslinked spherical nanoparticles with core-shell topology. *Advanced Materials*, 2000, **12,** 1899–1908. doi:10.1002/1521-4095(200012)12:24<1899::AID-ADMA1899>3.0.CO;2-T
7. Nalwa, H.S. (Editor), Handbook of nanostructured materials and nanotechnology: Synthesis and processing. vol. 1, San Diego, Academic Press 1999.
8. Edelstein, A.S. & Cammarata R.C. (Editor). Nanomaterials: Synthesis, properties and applications. Bristol, Institute of Physics Publishing 1996. doi: 10.1887/0750305789
9. Koch, C.C. Nanostructured materials: An overview. *In* Bulk Nanostructured Materials. Edited by M.J. Zehetbauer and Y.T. Zhu Weinheim. Wiley–VCH Verlag, 2009, pp. 3–20.
10. Chow, G.M.; Ambrose, T.; Xiao, J.; Kaatz, F. & Ervin, A. Nanostructured Co-Cu powders via a chemical route. *Nanostructured Materials* 1993, **2**, 131–138. doi: 10.1016/0965-9773(93)90017-6
11. van de Graaf, M.A.C.G.; ter Maat, J.H.H. Burggraaf, & A.J. Ceramic Powders: preparation, consolidation, and sintering. *In* Materials Science Monographs, Edited by P. Vincenzini Amsterdam, Elsevier 1983, pp 783–794.
12. Yano, K.; Nandwana, V.; Chaubey, G.S.; Poudyal, N.; Kang, S.; Arami, H.; Griffis, J. & Liu, J.P. Synthesis and characterization of magnetic FePt/Au Core/shell nanoparticles. *J. Phy. Chem. C*, 2009, **113**, 13088–13091. doi: 10.1021/jp901985u
13. Mukherji, D.; Pigozzi, G.; Schmitz, F.; Näth, O.; Rösler, J. & Kostorz, G. Nano-structured materials produced from simple metallic alloys by phase separation. *Nanotechnology*, 2005, **16,** 2176–2187. doi: 10.1088/0957-4484/16/10/034
14. Rösler, J. & Mukherji, D. Design of nanoporous superalloy membranes for functional applications. *Adv. Engineering Mat.*, 2003, **5**, 916–918. doi: 10.1002/adem.200300520
15. Pigozzi, G.; Mukherji, D.; Gilles, R.; Barbier, B. & Kostorz, G. Ni3Si(Al)/a-SiOx core–shell nanoparticles: characterization, shell formation, and stability. *Nanotechnology*, 2006, **17**, 4195–4203. doi: 10.1088/0957-4484/17/16/033
16. Veiseh, O.; Gunn, J.W. & Zhang, M. Design and fabrication of magnetic nanoparticles for targeted drug delivery and imaging. *Adv. Drug Delivery Rev.*, 2010, **62,** 284–304. doi: 10.1016/j.addr.2009.11.002
17. Kumar, C.S.S.R. & Mohammad, F. Magnetic nanomaterials for hyperthermia-based therapy and controlled drug delivery. *Adv. Drug Delivery Rev.*, 2011, **63**, 789–808. doi: 10.1016/j.addr.2011.03.008
18. Lópeza, M.B.; Teijeiro, A. & Rivas, J. Magnetic nanoparticle-based hyperthermia for cancer treatment. *Rep. Practical Onco. Radio.*, 2013, **18,** 397–400. doi: 10.1016/j.rpor.2013.09.011
19. Stephen, Z.R., Kievit, F.M. & Zhang, M. Magnetite nanoparticles for medical MR imaging. *Mater Today* (Kidlington), 2011, **14,** 330–338. doi: 10.1016/S1369-7021(11)70163-8
20. Ferrari, M. Cancer nanotechnology: Opportunities and challenges. *Nature Reviews: Cancer*, 2005, **5**, 161–171.
21. Belting, M.; Sandgren, S. & Wittrup, A. Nuclear delivery of macromolecules: barriers and carriers. *Adv. Drug Delivery Rev.*, 2005, **57**, 505–527. doi: 10.1016/j.addr.2004.10.004

22. Mogensen, T.H. Pathogen recognition and inflammatory signaling in innate immune defenses. *Clinical Microbio. Rev.,* 2009, **22,** 240–273. doi: 10.1128/CMR.00046-08
23. Longmire, M.; Choyke, P.L. & Kobayashi, H. Clearance properties of nano-sized particles and molecules as imaging agents: Considerations and caveats. *Nanomedicine,* 2008, **3**, 703–717. doi: 10.2217/17435889.3.5.703
24. Sonavane, G.; Tomoda, K. & Makino, K. Biodistribution of colloidal gold nanoparticles after intravenous administration: Effect of particle size. *Colloids Surfaces B: Biointerfaces,* 2008, **66**, 274–280. doi: 10.1016/j.colsurfb.2008.07.004
25. Choi, H.S.; Liu, W.; Misra, P.; Tanaka, E.; Zimmer, J.P.; Ipe, B.I.; Bawendi, M.G. & Frangioni, J.V. Renal clearance of quantum dots. *Nature Biotechnology,* 2007, **25**, 1165–1170. doi: 10.1038/nbt1340
26. Moghimi, S.M. Exploiting bone marrow microvascular structure for drug delivery and future therapies. *Adv. Drug Delivery Rev.,* 1995, **17**, 61–73. doi: 10.1016/0169-409X(95)00041-5
27. Banerjee, T.; Mitra, S.; Singh, A.K.; Sharma, R.K. & Maitra, A. Preparation, characterization and biodistribution of ultrafine chitosan nanoparticles. *Int. J. Pharmaceutics.* 2002, **243,** 93–105. doi: 10.1016/S0378-5173(02)00267-3
28. Moghimi, S.M. Mechanisms of splenic clearance of blood cells and particles: towards development of new splenotropic agents. *Adv. Drug Delivery Rev.,* 1995, **17,** 103–115. doi: 10.1016/0169-409X(95)00043-7
29. Davis, M.E. Non-viral gene delivery systems. *Current opinion Biotechnol.,* 2002, **13,** 128–131.
30. Chouly, C.; Pouliquen, D.; Lucet, I.; Jeune, J.J. & Jallet, P. Development of superparamagnetic nanoparticles for MRI: effect of particle size, charge and surface nature on biodistribution. *Journal Microencapsulation,* 1996, **13,** 245–255. doi: 10.3109/02652049609026013
31. Widder, K.J.; Morris, R.M.; Poore, G.A.; Howard, D.P. & Senyei, A.E. Selective targeting of magnetic albumin microspheres containing low-dose doxorubicin: total remission in Yoshida sarcoma-bearing rats. *Euro. J. Cancer Clinical Oncol.,* 1983, **19,** 135–139. doi: 10.1016/0277-5379(83)90408-X
32. Sun, C.; Lee, J.S.H. & Zhang, M.Q. Magnetic nanoparticles in MR imaging and drug delivery. *Adv. Drug Delivery Rev.,* 2008, **60,** 1252–1265. doi: 10.1016/j.addr.2008.03.018
33. McCarthy, J.R. & Weissleder, R. Multifunctional magnetic nanoparticles for targeted imaging and therapy. *Adv. Drug Delivery Rev.,* 2008, **60,** 1241–1251. doi: 10.1016/j.addr.2008.03.014
34. Dobson, J. Magnetic nanoparticles in MR imaging and drug delivery. *Nanomedicine,* 2006, **1**, 31–37. doi: 10.2217/17435889.1.1.31
35. Chen, S.; Wang, L.; Duce, S.L.; Brown, S.; Lee, S.; Melzer, A.; Cuschieri, A. & André, P. Engineered biocompatible nanoparticles for in vivo imaging applications. *J. Am. Che. Society,* 2010, **132,** 15022–15029. doi: 10.1021/ja106543j
36. Yi-Xiang, J. Wang. Superparamagnetic iron oxide based MRI contrast agents: Current status of clinical application. *Quantitative Imaging Medicine Surgery,* 2011, **1,** 35–40.
37. Na, H.B.; Song, I.C. & Hyeon, T. Inorganic nanoparticles for MRI contrast agents. *Advanced Materials,* 2009, **21**, 2133–2148. doi: 10.1002/adma.200802366
38. Gao, J.; Liang, G.; Cheung, J.S.; Pan, Y.; Kuang, Y.; Zhao, F.; Zhang, B.; Zhang, X.; Wu, E.X. & Xu, B. Multifunctional yolk-shell nanoparticles: A potential MRI contrast and anticancer agent. *J. Am. Chemical Society,* 2008, **130,** 11828–11833. doi: 10.1021/ja803920b
39. Mukherji, D.; Muller, R.; Gilles, R.; Strunz, P.; Rosler, J. & Kostorz, G. Nanocrystalline Ni_3Al-type intermetallic phase powder from Ni-base superalloys. *Nanotechnology,* 2004, **15,** 648–657. doi: 10.1088/0957-4484/15/5/042
40. Doi, M. TElasticity effects on the microstructure of alloys containing coherent precipitates. *Progress in Mater. Sci.,* 1996, **40,** 79–180. doi: 10.1016/0079-6425(96)00001-1
41. Kny, E. The methodology of phase extraction in nickel-base superalloys. *Practical Metallography,* 1976, **13,** 549–561.
42. Mukherji, D. & Pigozzi, G. Ultrastructure of core-shell nanoparticles by high-resolution electron microscopy. *Microscopy and Analysis,* 2007, **7,** 5–8.
43. Rösler, J.; Näth, O.; Jäger, S; Schmitz, F. & Mukherji, D. Fabrication of nanoporous Ni-based superalloy membranes. *Acta Materialia,* 2005, **53,** 1397–1406. doi: 10.1016/j.actamat.2004.11.038
44. Jonah Erlebacher. An Atomistic description of dealloying porosity evolution, the critical potential, and rate-limiting behavior. *J. Electrochemical Society,* 2004, **151,** C614–C626. doi: 10.1149/1.1784820
45. Parks, B.W.; Fritz, J.D. & Pickering, H.W. The difference un the electrochemical behavior of the ordered and disprdered phase of Cu_3Au. *Scripta Materialia,* 1989, **23,** 951–956. doi: 10.1016/0036-9748(89)90276-7
46. Pigozzi, G. TIntermetallic nanoparticles: synthesis and characterization. ETH Zurich, Switzerland 2006, PhD Thesis.
47. Mukherji, D.; Pigozzi, G. & Kostorz, G. Core-shell nanoparticles: Imaging and structure determination of the core and the shell regions. *Imaging Microscopy,* 2006, **8,** 15-16. doi: 10.1002/imic.200790025
48. Paulose, M.; Grimes, C.A.; Varghese, O.K. & Dickey, E.C. Self-assembled fabrication of aluminum–silicon nanowire networks. *Appl. Phy. Letters,* 2002, **81,** 153–155.

doi: 10.1063/1.1492005
49. Mukherji, D. & Pigozzi, G. Synthesis of siper paramagnetic nanoparticles of Ni_3Fe and Co_3Al intermetallics.
50. Figueroa, A.I.; Bartolomé, F.; Bartolomé, J.; García, L.M.; Petroff, F.; Deranlot, C.; Wilhelm, F. & Rogalev, A. Breakdown of Hund's third rule in amorphous Co-W nanoparticles and crystalline Co_3W alloys. *Physical Review B*, 2012, **86**, 064428-1–9. doi: 10.1103/PhysRevB.86.064428
51. Song, Y. & Jin, S. Synthesis and properties of single-crystal β 3 - Ni 3 Si nanowires. *App. Phy. Letters*, 2007, **90,** 173122-1–3. doi: 10.1063/1.2732828
52. Dutra, A.T.; Ferrandini, P.L.; Costa, C.A.R.; Gonçalves, M.C. & Caram, R. Growth and solid/solid transformation in a Ni–Si eutectic alloy. *J. Alloys Compounds*, 2005, **399,** 202–207. doi: 10.1016/j.jallcom.2005.03.039
53. Nash, P. & Nash, A. Ni-Si (Nickel-Silicon) in Binary Alloy Phase Diagrams, vol. 2, T. B. Massalski, H. Okamoto, P.R. Subramanian (eds), Ohio, ASM International 1986, pp. 1755–1756.
54. Van Dyck, S.; Delaey, L.; Froyen, L. & Buekenhout, L. Microstructural evolution and its influence on the mechanical properties of a nickel silicide based intermetallic alloy. *Intermetallics*, 1997, **5,** 137–145. doi: 10.1016/S0966-9795(96)00073-8
55. Zhang, H.L.; Li, F.; Liu, C. & Cheng, H.M. The facile synthesis of nickel silicide nanobelts and nanosheets and their application in electrochemical energy storage. *Nanotechnology*, 2008, **19**, 165606-1–7. doi: 10.1088/0957-4484/19/16/165606
56. Jang, J.S.C. & Tsau, C.H. Disordering of the Ni3Si intermetallic compound by mechanical milling. *J. Material Sci.*, 1993, **28**, 982–988. doi: 10.1007/BF00400883
57. Pigozzi, G.; Mukherji, D.; Gilles, R.; Jencus, P. & Siemers, C. The measurement of internal strain in core–shell Ni_3Si(Al)–SiOx nanoparticles. *Nanotechnology*, 2009, **20**, 245704-1–7. doi: 10.1088/0957-4484/20/24/245704
58. Rodríguez-Carvajal, J. Recent advances in magnetic structure determination neutron powder diffraction. *Physica B: Condensed Matter,* 1993, **192**, 55–69. doi: 10.1016/0921-4526(93)90108-I
59. Rietveld, H.M. A profile refinement method for nuclear and magnetic structures. *J. Appl. Crystallography*, 1969, **2,** 65–71. doi: 10.1107/S0021889869006558
60. Heenan, R.K. & Eastoe, J. Droplet interfacial structure studied by SANS contrast variation. J. Appl. Crystallography 2000, 33, 749–752. doi: 10.1107/S0021889800099854
61. Strunz, P.; Mukherji, D.; Pigozzi, G.; Gilles, R.; Geue, T. & Pranzas, K. Characterization of core-shell nanoparticles by small angle neutron scattering. *Applied Physics A*, 2007, **88**, 277–284. doi: 10.1007/s00339-007-4008-7
62. Pigozzi, G.; Mukherji, D.; Elerman, Y.; Strunz, P.; Gilles, R.; Hoelzel, M.; Barbier, B. & Schmutz, P. Effects of size reduction on the structure and magnetic properties of core–shell Ni_3Si/silica nanoparticles prepared by electrochemical synthesis. *J. Alloys Compounds* 2014, **584,** 119–127. doi: 10.1016/j.jallcom.2013.09.035
63. Sigfusson, T.I. & Lonzarich, G.G. Magnetocrystalline anisotropy in the weak itinerant ferromagnet Ni_3Al. *Physica Scripta*, 1982, **25,** 720–725. doi: 10.1088/0031-8949/25/6A/016
64. Chen, X.; Zhang, B.; Li, C.; Shao, Z.; Su, D.; Williams, C.T. & Liang, C. Structural and electrochemical properties of nanostructured nickel silicides by reduction and silicification of high-surface-area nickel oxide. *Materials Research Bulletin*, 2012, **47,** 867–877. doi: 10.1016/j.materresbull.2011.11.019
65. Himuro, Y.; Tanaka, Y.; Kamiya, N.; Ohnuma, I.; Kainuma, R. & Ishida, K. Stability of ordered L12 phase in Ni_3Fe–Ni3X (X:Si and Al) pseudobinary alloys. *Intermetallics*, 2004, **12**, 635–643. doi: 10.1016/j.intermet.2004.03.008
66. Himuro, Y.; Tanaka, Y.; Ohnuma, I.; Kainuma, R. & Ishida, K. Phase equilibria and g0-L12 phase stability in the Ni-rich portion of Ni–Fe–Si and Ni–Fe–Al systems. *Intermetallics*, 2005, **13**, 620–630. doi: 10.1016/j.intermet.2004.10.009
67. Pickering, H.W. & Wagner, C. Electrolytic dissolution of binary alloys containing a noble metal. *J. Electrochemical Society*, 1967, **114,** 698–706. doi: 10.1149/1.2426709
68. Masuda, H. & Fukuda, K. Ordered metal nanohole arrays made by a two-step replication of honeycomb structures of anodic alumina. *Science*, 1995, **268**, 1466–1468. doi: 10.1126/science.268.5216.1466
69. Chu, S.Z.; Wada, K.; Inoue, S. & Todoroki, S. Fabrication and characteristics of nanostructures on glass by Al anodization and electrodeposition. *Electrochimca Acta*, 2003, **48,** 3147–3153. doi: 10.1016/S0013-4686(03)00344-X
70. Schloesser, J.; Rösler, J. & Mukherji, D. Deformation behaviour of freestanding single-crystalline Ni_3Al-based nanoparticles. *Int. J. Materials Res.*, 2011, **102**, 532–537. doi: 10.3139/146.110504
71. Rösler, J.; Mukherji, D.; Schock, K. & Kleindiek, S. Forging of metallic nano-objects for the fabrication of submicron-size components. *Nanotechnology*, 2007, **18,** 125303-1–5. doi: 10.1088/0957-4484/18/12/125303

ACKNOWLEDGEMENTS

The idea of nanoparticles synthesis of intermetallic phases from metallic alloys is an extension of the ESPD process, which was originally developed and patented for the synthesis of nano-porous membranes. The German patent (DE 102 31 577.9-09) for the manufacture of nano-porous membrane is jointly held by the author and Professor Joachim Rösler, Head, Material Science Institute and Technische Universität

Braunschweig, Germany. The nanoparticle synthesis work was carried out at the Institute of Applied Physics, Swiss Federal Institute of Technology, ETH Zurich, Switzerland headed by retired Professor Emeritus of Physics, Gernot Kostorz. The author is grateful to both Professors for giving him the opportunity for this work and their support and guidance. The work of nanoparticle development was mainly carried out by Dr Giancarlo Pigozzi, as his PhD work at ETH Zurich under the guidance of the author and later at the Swiss Federal Laboratories for Materials Science and Technology, EMPA Dübendorf, Switzerland in collaboration with Dr Pigozzi and his contribution to this research is enormous and the author thanks him.

For the various characterisations of the different nanoparticles including the MNPs the researchers from many different institutions in Europe were involved and the author would like to express sincere thanks to each and every one of them. Researchers/Collaborators include: Dr Pavel Strunz and Dr Přemysl Beran, Nuclear Physics Institute, Rez near Prague, Czech Republic; Dr Ralph Gilles, Dr Michael Hofmann, and Dr Markus Hoelzel, Technische Universität München, Forschungs-Neutronenquelle Heinz Maier-Leibnitz (MLZ), Garching, Germany, helped in small angle neutron scattering (SANS) and neutron diffraction measurements. Dr Gerhard Schumacher, Helmholtz-Zentrum Berlin für Materialien und Energie, Berlin, Germany; Dr Ivo Zizak, Berliner Elektronenspeicherring-Gesellschaftfür Synchrotronstrahlung, Berlin, Germany; Dr Peter Jencus and Mr Carsten Siemers, IfW, TU braunsschweig for measurements at the synchrotron beamlines. Mr Bruno Barbier, Steinmann Institut, University of Bonn, Germany for X-ray diffraction measurements. Professor Yalçın Elerman, Department of Engineering Physics, University of Ankara, Turkey and Professor Mehmet Acet, Institute of Experimental Physics, University of Duisburg-Essen, Germany, for magnetic measurements.

CONTRIBUTOR

Dr Debashis Mukherji received BTech (H) and PhD (Metallurgical Engineering) from Indian Institute of Technology Kharagpur, India. Presently working as a Senior Scientist at the Technische Universitaet Braunschweig, Germany. Has expertise in vacuum melting, material characterization, electron microscopy, neutron scattering and x-ray, neutron and synchrotron diffraction. Main research interests include : Nano-structured material for bio medical applications and high temperature material for gas turbine. Having more than 150 publications in reviewed International journals. Currently working on the development of Co-Re-based alloys to supplement Ni-based superalloys for higher temperature application in gas turbines.